Lab on a Chip

PAPER

View Article Online
View Journal | View Issue

Cite this: *Lab Chip*, 2021, **21**, 3730

Expanding the limits towards 'one-pot' DNA assembly and transformation on a rapid-prototype microfluidic device†

James M. Perry, [ab] Guy Soffer, [bc] Raja Jain[ab] and Steve C. C. Shih *[abc]

DNA assembly and transformation are crucial to the building process in synthetic biology. These steps are significant roadblocks when engineering increasingly complex biological systems. To address this, recent development of widespread 'biofoundry' facilities has employed automation equipment to expedite the synthetic biology workflow. Despite significant progress, there is a clear demand for lower-cost and smaller-footprint automation equipment. The field of microfluidics have emerged to provide automation capabilities to meet this demand. However, we still lack devices capable of building large multi-gene systems in a consolidated process. In response to this challenge, we have developed a digital microfluidic platform that performs "one-pot" Golden Gate DNA assembly of large plasmids and transformation of *E coli*. The system features a novel electrode geometry and modular design, which make these devices simple to fabricate and use, thus improving the accessibility of microfluidics. This device incorporates an impedance-based adaptive closed loop water replenishment system to compensate for droplet evaporation and maintain constant assembly reaction concentrations, which we found to be crucial to the DNA assembly efficiency. We also showcase a closed-loop temperature control system that generates precise thermodynamic profiles to optimize heat shock transformation. Moreover, we validated the system by assembling and transforming large and complex plasmids conferring a biosynthetic pathway, resulting in performance comparable to those of standard techniques. We propose that the methods described here will contribute to a new generation of accessible automation platforms aimed at speeding up the 'building' process, lowering reagent consumption and removing manual work from synthetic biology.

Received 10th May 2021,
Accepted 28th July 2021

DOI: 10.1039/d1lc00415h

rsc.li/loc

Introduction

The field of synthetic biology is expanding quickly with new microbial strains engineered to produce a wide set of valuable products.[1–3] A rapid design–build–test cycle is vital to engineering strains which efficiently produce the desired heterologous metabolite. This starts with assembling diverse combinations of DNA parts and transforming them into a microbial factory such as *E. coli* or *S. cerevisiae*. Often the success of the engineering process in synthetic biology depends on the effectiveness of building and testing large libraries of genetic parts, and automation is an invaluable tool for this process. Microfluidics is becoming a common tool to expedite synthetic biology[4] by giving researchers the ability to build custom automation systems capable of handling complex workflows at low cost. By combining and automating lengthy protocols, these systems will ultimately minimize manual steps, which will then improve reproducibility while significantly reducing reagent and plastic consumption.

In particular, a variety of microfluidic formats have already been developed to tackle the challenge of DNA assembly such as laminar flow-based devices,[5–7] digital microfluidics (DMF),[8–10] and hybrid droplet–DMF devices.[11] The current best practices for microfluidic-based DNA assembly have yielded high-fidelity, two- or three-part assemblies.[5,11,12] However, these constructs are small (~3 kb) and essentially non-functional, whereas engineering complex biological systems for the development of vaccines, therapeutics, fuels and materials requires much larger (>10 kb), multi-part assemblies. The challenge with larger and more fragmented assembly reactions is that their uptake into *E. coli* is less efficient, making it difficult to obtain the desired construct.[13] Instead, engineers rely on multiple rounds of cloning (as well

[a] *Department of Biology, Concordia University, 7141 Sherbrooke Street West, Montréal, Québec, H4B 1R6, Canada. E-mail: steve.shih@concordia.ca; Tel: +1 (514) 848 2424 x7579*
[b] *Department of Electrical and Computer Engineering, Concordia University, 1455 de Maisonneuve Blvd. West, Montréal, Québec, H3G 1M8, Canada*
[c] *Centre for Applied Synthetic Biology, Concordia University, 7141 Sherbrooke Street West, Montréal, Québec, H4B 1R6, Canada*

† Electronic supplementary information (ESI) available. See DOI: 10.1039/d1lc00415h

as purification and sequence verification) to build their constructs.

After the assembly process, the DNA constructs are introduced into host cells. Methods like heat shock or electroporation are standard protocols for transforming large plasmids (>100 kb) into host cells.[14] There are several microfluidic platforms that have performed heat shock[15–17] or electroporation[11,18–20] protocols; however to date, there is only one device, developed by Shih *et al.*, which combines DNA assembly and electroporation-based transformation.[11] Shih and his colleagues constructed a custom hybrid droplet–DMF device to automate the widely-used Golden Gate assembly reaction as well as the transformation of assembled plasmids. Their device used a two-plate DMF device to combine and mix components of the assembly reactions. Next, droplets were moved through a channel where they were mixed with cells and passed through an electric field for electroporation. Although this work shows the advantages of microfluidic-based assembly and transformation, the performed assemblies were small (~3 kb) three-fragment plasmids containing *GFP* cassettes – not used directly for an application. Additionally, this work only performed the ligation step of the Golden Gate assembly reaction, with the digestion and purification conducted prior to device operation.

Coupling multi-part assembly with electroporation on microfluidics is challenging because the device has to provide an intense electric field to achieve optimal levels of transformation efficiency.[21] Bacteria and yeast survival drops significantly when exposed to electric fields higher than 15 kV cm^{-1} unless there is a channel geometry allowing for a field gradient.[18] Achieving the optimal electric field and channel geometry ultimately increases the fabrication demands (*i.e.* multi-layer photolithography relying on precise alignment tools) making the cost of these devices prohibitive. Instead of relying exclusively on electroporation to maximize the yield of assembled products, one approach is to focus on improving the efficiency of the assembly reaction. For Golden Gate assembly, this requires long periods of thermocycling.[22–24] For a microfluidic device, this means integrating closed-loop temperature control to enable thermocycling conditions, which can also be used for heat shock transformation. Temperature control systems can be built into the device apparatus rather than onto the individual microfluidic chip[17] making this approach more sustainable than on-chip electroporation.

Several recent DMF studies rely on a cleanroom-based fabrication process to pattern gold or chromium electrodes onto glass substrates.[15,16,25–27] Given the intricate and resource-dependent cleanroom fabrication procedures, several groups have developed simple, rapid-protoyping, fabrication techniques using printed circuit boards or conductive inks.[28–34] Using these highly accessible fabrication techniques enables easier entry of non-microfluidic experts to 'lab-on-chip' system development and encourages biologists to implement microfluidics into their own automation workflow.

We present a rapid prototype DMF system that expands the capabilities of DNA assembly and transformation and improves on several methods described by Shih *et al.* (2015).[11] These advances include: a modular device design approach which simplifies electrode routing demands and can be fabricated without a cleanroom technology. In addition, the device supports the first "one-pot" Golden Gate assembly performed using microfluidics. The device combines six DNA fragments into a 14 kb plasmid conferring the violacein biosynthesis pathway. After assembly, the device automates heat shock transformation of the assembled plasmid with heat shock temperature curves which have been optimized to boost transformation efficiency at the micro-scale. To fully support the assembly and transformation of large constructs on the device, we also have integrated a closed-loop water replenishing system to compensate for sample evaporation while performing several hours of thermocycled incubation thus addressing a longstanding limitation of DMF. Our new low-cost and user-friendly system offers a combined automated assembly–transformation process, expanding the limits of DMF-driven synthetic biology.

Materials and methods

Device fabrication

Device designs were made using AutoCAD. The block designs of the electrodes enabled 'copy-and-paste' functionality. The designs were printed using an HP Laser Jet 3015 printer onto transfer paper (Abra Electronics cat no. TTP-10). The printed toner was transferred onto PCB substrates (Digikey cat no. 50-1507) using a laminator (Tamerica cat no. SM-330) with the design face-down on the copper substrate. During the toner transfer process, the PCBs were rotated 90° after each passed through the laminator to ensure equal heat transfer. This process was completed in no less than 7 minutes in order to adequately transfer the toner to the copper. The transfer paper was removed by submerging the PCBs in warm water (~50 °C) and gently peeling back the paper. After that, the boards were inspected for areas where the toner did not transfer properly. For areas missing toner, toner touch-up was done using a Staedtler Red Lumocolor Fine Tip pen (Abra Electronics, Montréal, QC) which has an ink resistant to the copper etchant. The boards were immersed in ferric chloride (MG Chemicals cat no. 415-4 L) for 10 min at 180 °C with constant agitation to remove the exposed copper. Acetone was used to remove the toner from the etched PCBs. The devices were verified using a table-top microscope to check for short circuits or joined electrode gaps. Any short circuits between electrodes were removed using a razorblade when possible. Prior to device operation, ITO glass was cut to the width of the electrodes using a diamond glasscutter. 100 μL of Fluoropel Cytonix was pipetted onto the ITO-coated side and spin-coated for 30 s at 1500 rpm. Fluoropel was also applied to the ITO glass edges. To apply a dielectric to the PCB, 20 μL of polydimethylsiloxane oil was pipetted onto the

PCB surface and a square of Parafilm-M was stretched over the PCB and secured on the back by self-adhesion of the Parafilm-M and excess Parafilm-M was trimmed from the back. The oil created a seal between the PCB surface and the Parafilm-M eliminating any air pockets that prevented a firm seal between the device and the Parafilm. Additionally, a small amount of oil was applied to the Parafilm surface by first, pipetting a 50 μL droplet of water on the device, adding <0.5 μL of oil to the droplet, and then using the droplet to 'paint' the surface of the device by tilting the device side to side. After trimming excess Parafilm from the back of the device, double-sided tape with a thickness of ~90 μm was used to secure an ITO top-plate above the device surface. The pogo pins of the in-house automation setup (see https://bitbucket.org/shihmicrolab/james_m._perry_dmf/) were adequate to puncture the Parafilm-M at the point of connection to the PCB contact pads.

DNA assembly

Fragment preparation. All primers were designed using Benchling software with predicted T_m values centered at 55 ± 1 °C using default T_m calculation parameters. This consistently resulted in an optimum annealing temperature of 65 °C. To generate fragments for Golden Gate assembly, primers contained a 5′ BsaI/Eco31I recognition site. For each DNA part, four 50 μL PCR reactions (see Table S1† for reaction components and volumes) were setup using Phusion DNA polymerase (Thermo Fisher cat no. F530S) with the PCR conditions in Table S2.† To remove methylated template DNA from each reaction, 1 μL of DpnI (Invitrogen cat no. IVGN0106) was added to each 50 μL PCR product and incubated for 2 h. The PCR products were verified by gel electrophoresis and purified using a gel extraction kit (BioBasic).

Benchtop Golden Gate reactions. For cloning reactions, a 15 μL Golden Gate master-mix was prepared containing 2.5 μL T4 DNA ligase buffer (NEB cat. no. B0202S), 2 μL Eco31I (10 U μL^{-1}) (Invitrogen cat no. IVGN0366), 0.5 μL T4 DNA ligase (5 U μL^{-1}) (Invitrogen cat. no. EL0011), and 5 μL of DI water. NEB T4 ligase buffer and Invitrogen T4 ligase were selected since this combination provided optimal droplet movement on the digital microfluidic platform. The buffers and enzymes from both suppliers are interchangeable without noticeable differences in activity. Golden Gate reactions were made by combining 3 μL of DNA fragment solution containing 40 fmol of each DNA fragment and 2 μL of the Golden Gate master-mix to bring the volume to a total of 5 μL. This reaction was thermocycled as described in Table S3.† See plasmid maps for assembled pFAB constructs in Fig. S1.†

Benchtop transformation of the assembled product. For benchtop transformation controls, see Table S4† for conditions. Briefly, the benchtop (5 μL) or device (~1.25 μL) assembly product was added to 50 μL competent cell aliquots. The aliquots were then placed in a 42 °C water bath for 30 s. The cells were then placed in an ice bath for three minutes. After that, the sample volume was brought to 1000 μL with SOC media, followed by an hour of recovery at 37 °C at 200 rpm. The samples were plated on LB-Kan plates and placed at 37 °C overnight.

Violacein plasmid construction. The violacein plasmid construction is shown in Fig. S2.† The sequences for five T7 promoter variants were designed following Jones *et al.* (2015).[35] For this work, the T7 promoters were designed as 141 bp fragments which include A) a 20 bp barcode region used to identify the 5′ end of each promoter variant and B) the T7 promoter containing a 5 bp variable region of either C4, TCAAG; consensus, TAGGG; H10, CGGAA; H9, ATACT; or G6, TTTCG. The fragments were constructed using overlapping forward and reverse oligo pairs (VJ_55-64; see Table S5†). The overlapping region represents an annealing temperature of 65 °C. These oligos were combined and amplified using the PCR conditions in Table S2.† An additional PCR reaction was performed to apply 5′ BsaI/Eco31I recognition sites to each fragment using primers VJ_5-12. Violacein gene fragments (total of 5 – Vio A, B, E, C, D) were amplified from pETM6-vioABECD using primers VJ_13-22. An entry vector for the violacein assemblies was constructed by amplifying pETM6-vioABECD, excluding the original violacein gene cassettes and the ampicillin resistance cassette. The ampicillin resistance cassette of pETM6 (which contains an internal BsaI/Eco31I site which could affect the Golden Gate assembly performance) was replaced with a kanamycin resistance cassette from pFAB4876 to form a new entry vector called pETVJ. This was done by Golden Gate assembly of fragments amplified from pETM6 (using primers VJ_1 and VJ_2) and pFAB4876 (using primers VJ_3 and VJ_4). The entry vector pETVJ was then amplified with primers VJ_5 and VJ_6 to add 5′ BsaI/Eco31I sites. A plasmid promoter–violacein cassette library was constructed by combining promoter, gene and entry vector fragments using Golden Gate. This cassette library consists of the 25 combinations of violacein genes and T7 promoter variants. From this library, a selection of cassettes was amplified using primers VJ_25-54 and combined with a pETVJ fragment amplified from pETVJ with primers VJ_23 and VJ_24 to create violacein pathway plasmids. Specifically, cassettes Cons-VioA, Cons-VioB, Cons-VioE, Cons-VioC, and Cons-VioD and H10-VioA, H10-VioB, H9-VioE, H9-VioC, and G6-VioD were selected to build two contrasting pathways to avoid biasing one set of fragments during assembly.

Heat shock characterization tests

Different heat shock time and temperature combinations were performed to examine their effects on transformation efficiency (Fig. S3†). 10 ng of pUC19 plasmid DNA (mini-prepped) was added to 50 μL competent cell aliquots at a concentration of 0.2 ng μL^{-1} w/v and placed on ice. 1.5 μL aliquots were then placed in either 37 °C, 42 °C, or 47 °C water bath for either 15, 30, and 45 s. The cells were then

placed on ice for three minutes followed by an hour of recovery at 37 °C, and shaken at 200 rpm with 950 μL of SOC media. The cells were plated on LB-amp plates and placed at 37 °C overnight. Next, we measured the temperature curves in microcentrifuge tubes containing 100–400 μL of water using an NTC thermistor temperature sensor placed in the tubes shown in Fig. S4A.† Each tube was put through the heat shock protocol and the resulting temperature curves were fitted with the formulas shown in eqn (S1) and (S2)† using time constants (τ), which resulted in the highest R^2 score. Using these curves, an analytical model was built to determine time constants based on volume, as well as temperature maxima and minima to approximate the time constant for a standard 50 μL sample (Fig. S4B†).

Device transformation optimization

Triplicate samples comprised of ice-cold 0.8 μL of competent cells with 0.2 ng μL^{-1} pUC19 and 0.05% w/v Pluronic F-68 were pipetted onto the edge of the device ITO top plate and actuated into the reservoirs of the device. The samples were heat shocked using the integrated temperature control system[17] described in the ESI.† Eight different heat shock temperature profiles, differing in time constants (τ = 0.5, 10, 17, and 20 s) and T_{max} of either 37 °C or 42 °C, were implemented on the device. In each experiment, the temperature profile was calculated in real time every 0.5 s using eqn (S1)† (for the rise time) and eqn (S2)† (for the decay time) for 100 s. The calculated temperature value at each time point was used as the new setpoint of the temperature controller (PID algorithm). After heat shock, the samples were transferred to tubes containing 200 μL of SOC media and recovered at 37 °C for 1 h. Following recovery, the samples were plated on LB-agar containing ampicillin and incubated overnight at 37 °C. The transformation efficiency (CFU μg^{-1}) was calculated for each time constant.

On-device one-pot assembly and transformation

Optimization of DNA assembly using a volume replenishment system. A detailed description of the volume replenishment system used to limit the effects of sample evaporation on the device is described in the ESI† and depicted in Video S1. To validate the use of the volume replenishment system, 1250 nL assembly mixtures containing 8 fmol μL^{-1} pFAB fragments were pipetted onto the device. The samples were thermocycled using the schedules listed in Table S3† for either 5, 15 or 25 cycles. For each set of cycling conditions, the samples were either continuously replenished with water using the automated volume replenishment system or left to evaporate. The samples were then transferred into 50 μL competent cell aliquots, incubated on ice for 10 minutes followed by a 30 second heat shock at 42 °C and a 3 minute cool-down on ice. After heat shock, the samples were transferred to tubes containing 950 μL of SOC media and recovered at 37 °C for 1 h. After recovery, the samples were plated on LB-agar containing kanamycin and incubated overnight at 37 °C. The transformation efficiency (CFU μg^{-1}) was calculated for each sample and the measurements were performed in triplicate. As comparison to device assemblies, 5 μL benchtop samples were prepared and placed in a thermocycler using the same temperature schedules followed by transformation (as above).

Combined assembly and transformation. For on-device assemblies, each DNA fragment was adjusted to 40 fmol μL^{-1} for pFAB plasmid assembly and 150 fmol μL^{-1} for pETM6-Vio plasmid assembly. Prior to fluidic operation, the device's temperature was brought to 10 °C to limit evaporation. To bring reagents onto the device, 1.3 μL of each assembly component was pipetted onto the edge of the ITO glass and was loaded into the reservoir electrodes by applying a driving potential of 250 V_{RMS} at 15 kHz to draw the fluid into the reservoir. See Video S2† for the full automation assembly and transformation procedure on the device.

A device workflow for the 3-part pFAB assembly is shown in Fig. S5.† Briefly, droplets (~250 nL) of each DNA fragment and two droplets of the Golden Gate master mix were dispensed by pulling and necking as described previously[36] and actuated to the reservoir electrodes in the incubation region (Fig. 1A). The volume bit-value setpoint for each combined assembly sample droplet was established by measuring the volumes as described in the ESI.† This initial measurement value was used as a setpoint by the volume replenishment system to maintain the same volume for the rest of the procedure.

For the violacein pathway assembly, 6 droplets of pVJM6-Vio fragment samples (6 different fragments) and 2 droplets of the assembly master-mix were actuated to a reservoir electrode in the incubation area. The setpoint was established for the volume of 3 DNA fragment droplets and 2 master-mix droplets (~1250 nL) to ensure 8% Eco31I, 2% T4 ligase and 10% buffer concentrations for the reactions. To remove excess volume, the violacein assembly reactions were evaporated by heating to 37 °C until the setpoint was reached.

For both pFAB and pETVJ-Vio plasmid assemblies, the samples were then thermocycled on-device (using conditions in Table S3†). Throughout thermal cycling, the volume replenishment system (see the ESI† for details) was active to maintain the initial volumes of the assemblies which represent optimal concentrations of each reaction component. Benchtop reactions with a total volume of 5 μL were also made and thermocycled using the same schedules for comparison.

Assembly product concentration adjustment. To prepare the assembly products for transformation, each ~1250 nL sample was evaporated down to ~100 nL by heating to 37 °C for 10 minutes (see Fig. S5† for device operation assemblies). To improve the transformation efficiency of the assembled products on the device, 1/5 or 1/10 of the assembly reaction was prepared using the DMF device. The workflows for this are shown in Fig. S6.† Briefly, to prepare a 1/5 dilution (*i.e.* 1/5 of assembly DNA concentration) of an assembly product,

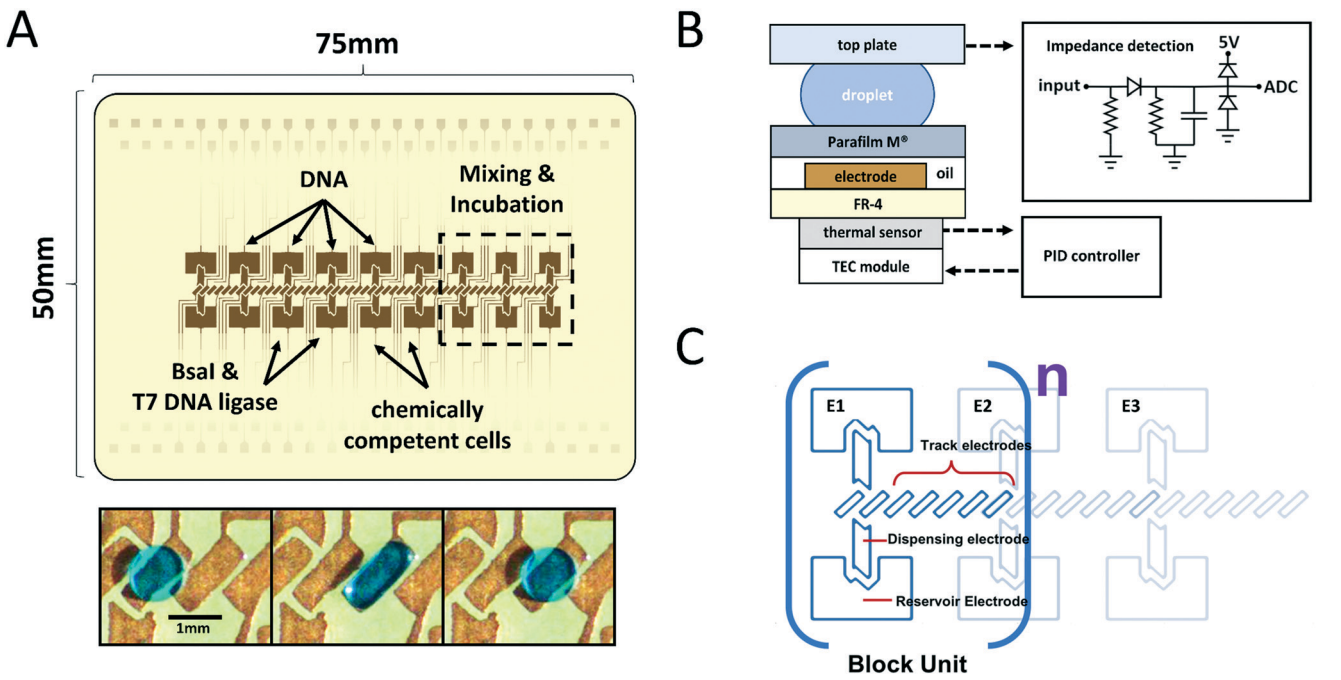

Fig. 1 Modular DMF design for assembly and transformation. A) DMF device fabricated using rapid-prototyping techniques. The device contains regions for storing and dispensing reagent droplets used for Golden Gate assembly such as DNA fragments and a master mix containing Eco31I (BsaI isoschizomer), T4 DNA ligase and 10× T4 DNA ligase buffer. Droplets are actuated to and mixed at incubation electrodes for thermocycling or transformation. The device also features a novel slanted electrode shape for optimized droplet movement and for reproducible device fabrication. The three-image pane below the device depicts a droplet moving between two electrodes. B) The side profile of the device's layers. An ITO top-plate connects the device to a grounded impedance detection circuit which is used to measure the relative volumes of liquid present at electrodes. An aluminium block housing an NTC thermistor connects the DMF chip to a TEC module used for temperature management using a PID algorithm. C) The design of the device is organized into modular sections called block units. Each block unit contains the necessary functions to dispense a droplet and move it along a section of the track. These block units take up the same horizontal space as their connecting contact pads making the addition of more blocks easy to implement in CAD design software.

one droplet was dispensed and reserved while the remaining product was actuated onto the electrode track and delivered to a waste electrode containing a Kimwipe wick. The initial single droplet was then moved back into the incubation electrodes. To prepare a 1/10 dilution (*i.e.* 1/10 final DNA concentration), three droplets of the product were discarded, followed by the merging of two droplets of water, and followed by dispensing two droplets to waste. After dilution, each sample was left to evaporate to less than ~250 nL at 37 °C. In all cases, the assembly product was left to evaporate prior to transformation to limit dilution of the competent cell mixture. pFAB constructs were used to compare assembly concentrations. pVio constructs used the 1/5 assembly product for transformation.

Transformation. Chemically competent cell aliquots were supplemented with 0.05% w/v Pluronic F-68. The on-device temperatures were brought to 0 °C. A 1.3 μL droplet of competent cells was pipetted onto the edge of the ITO glass (using pipette tips kept at 4 °C) and loaded into the reservoir electrodes by applying driving potentials to draw the fluid into the reservoir. Four droplets of cells were then dispensed from the reservoir and merged with each assembled and diluted product in their respective incubation electrode. The cells and the assembly products were mixed and incubated for 30 minutes at 0 °C. A heat shock protocol (time: 30 s, τ = 17 temp: 37 °C) was applied to the incubation region containing the transformation mixtures followed by 3 minutes of incubation at 0 °C. The droplets were removed from the device and pipetted into 200 μL of SOC followed by an hour of recovery at 37 °C with 200 rpm shaking. The cells were then plated on LB-kanamycin agar plates and placed at 37 °C overnight. The following day, colonies were counted on each plate.

For the pETVJ-VIOABECD assemblies, the plates were incubated for 2 days resulting in purple-coloured colonies, which were counted. Three purple colonies from pETVJ-Vio[4,4,4,4,4] and pETVJ-Vio[3,3,2,2,1] were inoculated into 5 mL of LB-kanamycin to prepare an overnight culture for plasmid purification. The pETVJ-Vio plasmids were then transformed into BL21-DE3 and plated on LB-kanamycin agar plates containing 1 mM IPTG. The plates were incubated overnight at 37 °C.

For pFab sequencing preparation, 4 colonies were chosen randomly from each plate and inoculated into 5 mL of LB-kanamycin to prepare an overnight culture for plasmid purification. The DNA samples were sent for Sanger sequencing (CHU de Québec-Université Laval Research Centre, QC). For alignment, ab1 files were converted to FASTA

format (QV > 20) using DNA Baser Assembler ver. 4 (DNA Sequence Assembler v4 2013 Heracle Biosoft SRL, http://www.DnaBaser.com). FASTA-format sequences were aligned using Blast2 (https://blast.ncbi.nlm.nih.gov/Blast.cgi) to three 100 bp regions centered around the location of assembly junctions for each pFab plasmid.

Results and discussion

Modular DMF design and fabrication

Digital microfluidics is an emerging platform ideal for biology[25,26] because it provides suitable capabilities for automating biological protocols. However, widespread adoption of this technology is hindered by the challenges of device design and cleanroom-based fabricated methods. There have been recent developments to simplify device prototyping (*i.e.* rapid prototyping). Yet, there remains two key limitations: 1) expensive dielectric materials (Parylene-C or SiN_3) or hydrophobic layers (Teflon-AF or Cytop) are still used on the rapid prototype devices, preventing reusability[32] and 2) each device has customized networks of electrodes, which require new routing across different designs.[37]

Here, we demonstrate a digital microfluidic device with a simplified design which is easy to fabricate. As shown in Fig. 1, we made use of commercially available copper boards (830 μm thick FR-4 with 100 μm thick copper) with electrodes patterned by PCB fabrication techniques.[28,32,33] In our case, the electrode pattern was printed onto toner-transfer paper and transferred to the copper board *via* heat lamination, followed by ferric chloride etching. Prior to use, the devices were coated with a thin layer of silicone oil to create an air-tight seal between the Parafilm M™ (*i.e.* dielectric and hydrophobic layer) and the PCB surface. We used devices fabricated in this manner to actuate droplets between two plates, without needing the separate hydrophobic (*e.g.* Teflon-AF) and dielectric layers (*e.g.* Parylene-C or SiN_3 requiring cleanroom-based deposition) (Fig. 1A, top view and B, side view). This approach is different from previously reported PCB-based digital microfluidic fabrication.[28,32,33] The novelty with our technique is that we can remove the Parafilm M™ dielectric and re-apply it between device uses – unlike the Parylene-C or SiN_3 coating. These devices are highly reusable and therefore, we only used a single fabricated PCB device for all experiments described in this work. The design is also simple to fabricate *via* commercial PCB manufacturing services for the purpose of mass production. With this approach, DMF-based biology becomes dramatically more accessible.

The traditional design of a DMF device consists of a network of electrodes arranged to suit the specific biology-related application. For each new electrode pattern, the designer must create individual wiring paths to each respective contact pad, which connects to the actuation voltage source. Creating these wiring paths can be complicated and tedious even with auto-routing features of PCB CAD software. When integrating automation with DMF,[25,26,36] the user must also create a map of the electrode pattern to the correct switches in the software, which are used to control electrode actuation. As shown in Fig. 1C, we sought to improve this challenge by standardizing the electrode layout into units called "blocks". Each block includes an optimized and reliable electrode signal routing that is also aligned with the chip's surrounding contact pads, which eliminates the burden of routing each individual electrode over the entire electrode array. Specifically, we created three functional blocks consisting of reservoir, dispensing, and track electrodes, which are used for standard droplet operations (*i.e.*, dispense, move, merge, and mix) for automating biological processes.[25,38] The designer can choose how many blocks are required for their device and link them end-to-end in AutoCAD (or PCB layout tools). We also designed python-based automation software using a modular object-oriented architecture (see BitBucket registry). The user interface consists of three main functions: dispense, track, and deliver (Fig. S7†). The user can change an element in the block and duplicate the change across the whole device, as well as easily update the software interface. For example, when mapping electrodes to the switches within the automation software, the layout of the first modular block presents all the information needed to expand the mappings to subsequent blocks by simply repeating the pattern and calling each function by block number. Structuring the device layout in a modular way not only improves scalability in terms of both hardware and software, but also simplifies the building and operation of the DMF device by ensuring that it is based on reliable and validated building blocks in both hardware and software domains. This is extremely important for both expert and non-expert users.

Another new feature is the simplified electrode shapes that enable reproducible rapid fabrication and high-fidelity droplet dispensing and movement. Cleanroom based DMF devices are conventionally designed with square electrodes,[8,11,26] or interdigitated electrodes, which improve droplet movement fidelity.[25,34,38] Initial experiments with square electrodes resulted in poor reproducibility in fabrication (~50% of devices were successful without defects) and were unable to successfully move droplets (0% of droplets were capable of actuation along a linear track) (Fig. S8†). One of the reasons for this poor fidelity is that the resolution of the printer and toner transfer process does not support gap distances lower than ~200 μm between electrodes. We observe that droplet boundaries tend to stay at the edge of the electrode where the electric field of an adjacent electrode is not strong enough to pull. Additionally, increasing the actuation potential (>400 V_{rms}) does not improve movement without also posing a risk of damaging the device components. In response to this, we interdigitated electrodes based on previous literature studies.[25,34,38] Interdigitation is a popular method to facilitate rapid droplet movement because it increases the droplet's contact with adjacent electrodes, which leads to more reliable droplet movement. In our case, interdigitation facilitated near perfect

droplet movement fidelity (and with a much lower applied voltage ~200 V_{rms}). However, the devices fabricated with this type of electrode commonly exhibit connected electrodes (~70%) due to the low resolution of PCB fabrication as compared with photolithography. Our solution was to implement a novel slanted-rectangle electrode shape which makes a half-herringbone pattern (Fig. 1). When a droplet is actuated, it stretches and conforms to the electrode. When the electrode is not actuated, the droplet forms a spheroid – in contact with adjacent electrodes and ready for subsequent movement (see Videos in the ESI†). The main difference between our design and the interdigitated design (*e.g.* Shih *et al.* (2013)[39]) is that our new shape reduces the number of interdigitated features between electrodes from two to one, resulting in fewer corners and edges while still enabling requisite droplet overlap with adjacent electrodes. As described in Fig. S8,† the fabrication of these devices resulted in low defect instances during fabrication (an average of 2 ± 2 connections per chip (~2%) required repair by hand) and excellent droplet movement across the linear electrode track at lower voltages (~200 V_{rms}). Hence, this electrode design was used for devices automating DNA assembly and transformation experiments. We propose that this simple electrode design will become a new standard – as simple as square electrodes and replacing overly complex interdigitation.

DNA assembly and transformation development on DMF

To demonstrate the capabilities of our rapid-prototype DMF device, we applied it to Golden Gate assembly and transformation. An overview of our DMF system setup is presented in Fig. S9.† Previous microfluidic-based Golden Gate assembly work automated the ligation of DNA fragments which were digested and purified off-chip.[6,11] Yet, the modular cloning (MoClo) standard,[23,24,40,41] which consolidates digestion and ligation into a single "one-pot" reaction, is increasingly common in the synthetic biology community. Performing a one-pot Golden Gate assembly requires mixing DNA parts, a ligase, a type IIS endonuclease and a reaction buffer followed by thermal cycling temperatures between 16 and 37 °C. To automate these

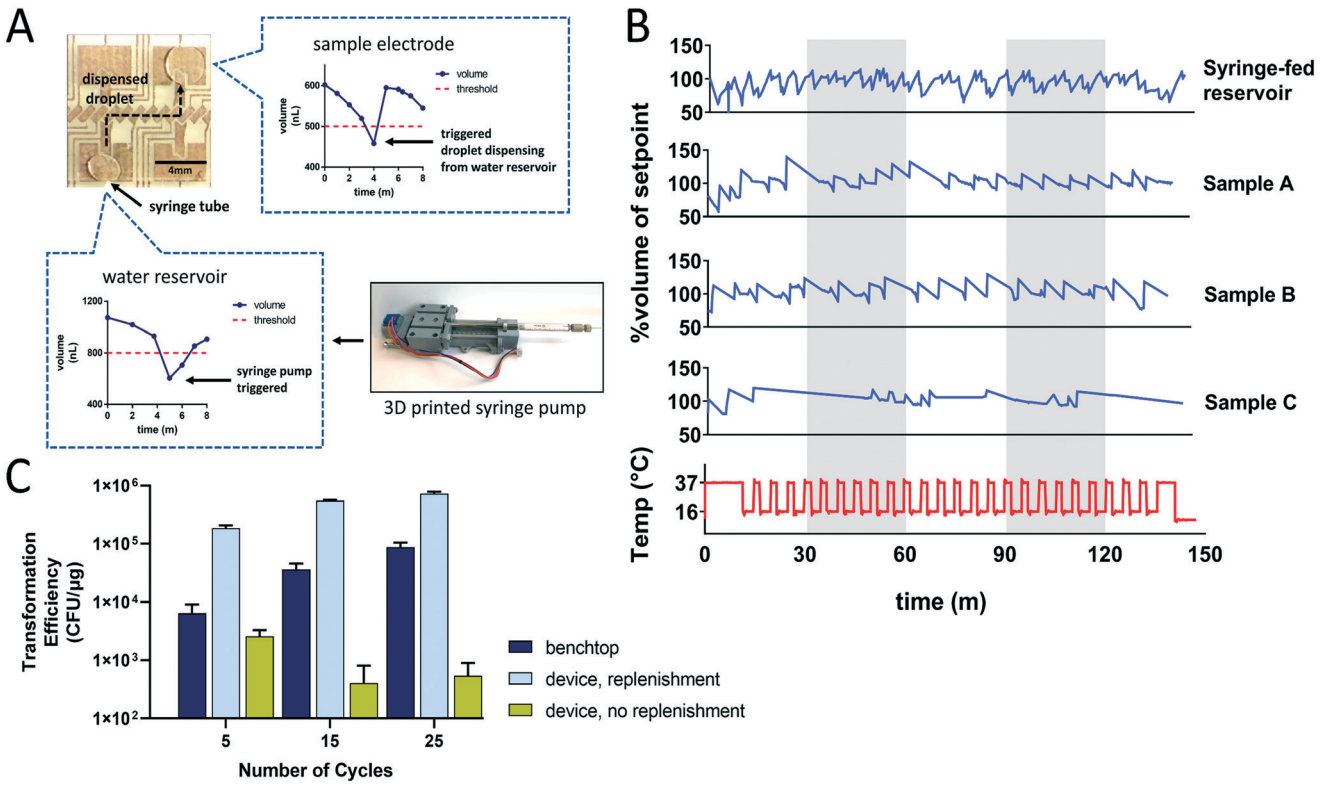

Fig. 2 Water replenishment system. A) Overview of a fully autonomous water replenishment system used to restore water content in continually evaporating samples. Using impedance to track the liquid volume, a setpoint value is established for each electrode hosting a sample. When sample volumes evaporate below a given threshold (equal to the setpoint minus half the volume of an average dispensed droplet) a new droplet is dispensed from a water reservoir electrode. The water reservoir is fed by a 3D-printed syringe pump system controlled by a PID algorithm using electrode impedance values as feedback to stabilize the flow rate. Excess water is removed from the reservoir by dispensing to the reservoir directly across from it which also contains a small piece of Kimwipe tissue to wick away the collected water over time. This wick system ensures that excess water does not buildup and interfere with normal droplet dispensing. B) Comparing the volumes of three samples during Golden Gate thermocycling performed on the device for 25 cycles (~150 min). C) Comparing the efficiency of Golden Gate assembly using 5, 15, and 25 cycles between 16 and 37 ° C using either a thermocycler or device with and without replenishment. Each data point represents at least three replicate measurements, and error bars represent ± SEM.

protocols on-device, we integrated a temperature control system resembling a thermocycler into our DMF setup, using a TEC module integrated below the device (described in our previous work[17]). To counteract the sample volume loss due to evaporation throughout thermocycling, we implemented an impedance-based feedback system, which triggers water replenishment to samples from a syringe pump-fed reservoir. There are many DMF systems that have integrated heaters[42–44] or impedance sensing.[39,45,46] However, this is the first successful demonstration (to our knowledge) of a DMF device that integrates both components and performs one-pot Golden Gate assembly and transformation.

Sample evaporation is a continuous challenge to digital microfluidics because the samples are exposed to the external environment. Although including oil as a filler medium may reduce these effects,[8,11,47] evaporation will still impact processes like DNA assembly when samples are heated for several hours. A solution to evaporation is to continuously re-supply samples with water to maintain the initial reaction concentrations. On our device, sample volumes are monitored using impedance sensing which is used to determine when the sample volumes fall below a threshold limit (Fig. 2A; Video S1†). The water reservoir is kept full using a syringe pump, which is interfaced to the device using capillary tubing. With the impedance system measuring the volume, we achieve excellent linearity and correlation with pipetted water samples and an average difference of ~3.1% in volume for the same device with different films (Fig. S10†). We implemented the replenishment system under thermocycling conditions. Fig. 2B shows three sample volumes (1250 nL) thermocycled 25 times between 16 and 37 °C for a total incubation time of 150 min (mimicking the temperature schedules for MoClo assembly;[24] Table S3†). As shown, the replenishment system was able to maintain the samples at ~±8.2% of their initial volumes (time-weighted trapezoid-rule), which is similar to our simulated model of the replenishment system, which was designed to fluctuate above and below a single droplet volume (250 nL) (Fig. S11†). This is a crucial feature, since thermocycling samples for hours results in significant amounts of water loss from samples, reducing the reaction efficiency (Fig. 2C). To demonstrate our replenishment system, we performed assemblies of pFAB plasmids (Fig. S1† for plasmid map) on the device using different numbers of cycles and compared the effect with and without the replenishment system and to a reaction performed in a standard benchtop thermocycling system. Fig. 2C shows that supporting longer Golden Gate reactions (*i.e.*, more cycles) on the device significantly improves the transformation efficiency of the assembled product by at least one order of magnitude. Specifically, when we conducted five cycles on the device, the efficiency is the highest on the device with replenishment (1.86×10^5 CFU μg^{-1}) compared to those without replenishment (2.57×10^2 CFU μg^{-1}) and using a benchtop thermocycler (6.43×10^3 CFU μg^{-1}) ($N = 3$). When increasing the number of cycles to 25, the efficiency dramatically improved on the device with replenishment (7.30×10^5 CFU μg^{-1}) in contrast to the device without replenishment (5.41×10^2 CFU μg^{-1}) and the benchtop thermocycler (8.71×10^4 CFU μg^{-1}). Generally, assemblies performed on the device without replenishment gave very few colonies (~3). We hypothesize that the assemblies on device with replenishment performed better than the assemblies on device without replenishment because the loss of water changes the concentration of the reaction components. Likewise, the benchtop thermocycler assemblies, which did not perform as well as samples replenished on DMF, had condensation on the side of the tubes post-incubation, indicating evaporation. This suggests that the manufacturer-recommended concentrations of components during thermocycling (such as T4 buffer) should be maintained with replenishment. Without such a system, Golden Gate assembly on a DMF (or any microfluidic) platform is impractical for large or multi-fragment plasmids since sample evaporation significantly reduces reaction efficiency.

After developing a platform for Golden Gate assembly, we turned our attention to the process of transformation. The traditional benchtop heat shock transformation protocol consists of placing the competent cells and plasmid in an ice bath and then raising the temperature to the commonly used 42 °C for 45 seconds and returning the mixture of cells and plasmid to the ice bath (Fig. 3A). The size and surface-to-volume ratio of DMF microscale samples typically result in a significantly different thermodynamic response compared to benchtop tube samples during the heat shock process. In the initial experiments, we experienced very low (or even zero) transformed colonies when performing transformation using the above parameters on the device. This led us to examine the temperature profile in a tube (by placing the temperature sensor inside the tube and using a thermocycler). In the tube, the standard heat shock protocol has a response profile exhibiting a slow increase towards the water bath temperature, yet never reaching the target of 42 °C within 30 seconds, followed by a slow descend towards the ice bath temperature resulting in a time constant τ of 17.7 seconds for a 50 μL sample (Fig. 3A). This observation was unexpected and compelled us to explore a heat shock landscape and its effects on the transformation efficiency in the tube and on the device.

To explore the effect of the heat shock temperature profiles, we first conducted benchtop optimization and extrapolation of the heat shock time constant for our target benchtop volume of 50 μL. Using an exponential fit, we determined that the 50 μL benchtop samples had a time constant of 17.7 seconds (Fig. S4†). Using the same time constant, we implemented the heat shock profile determined from the benchtop to the device by slowing down the rise time of the TEC module (COMSOL model verification shown in Fig. S13†). As a first test, we explored a heat shock protocol of 42 °C for 30 seconds on the device. As shown in Fig. 3B, the transformation efficiency on the device is higher with τ = 17 seconds compared to that with the default time constant (τ = 0.5 seconds). To improve the efficiency on the device

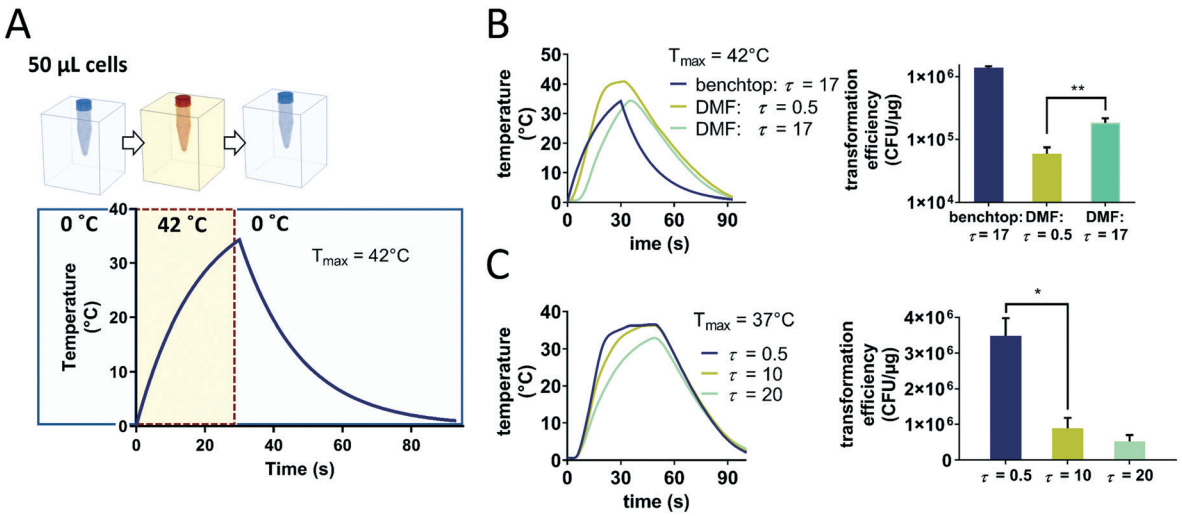

Fig. 3 Examining time constant effects on transformation. A) Overview of the typical heat shock protocol for transforming *E. coli* with plasmids using a microcentrifuge tube and temperature-regulated water baths. The resulting temperature curve for the protocol depicted below. This curve was generated by using a temperature sensor placed inside microcentrifuge tubes and fitted to thermodynamic formulas (see the Materials and methods section). Optimization of the heating profile on the device at two different temperatures: B) 42 °C and C) 37 °C. A dynamic setpoint method was used to mimic the heat transfer observed in microcentrifuge tubes. Changing temperatures as per the heat shock schedule depicted in A) using a TEC-based method on the device results in higher temperatures due to more rapid heating (τ = 0.5 seconds, see the line graph). When applying a gradually increasing setpoint (τ = 17 seconds), a similar heating profile (line graph) was achieved resulting in significantly higher transformation efficiencies ($p < 0.001$; bar graph). When exploring the new temperature control capabilities, it was found that a lower maximum setpoint (37 ° C as opposed to 42 °C) and a fast temperature rise time (τ = 0.5 second) yield significantly improved efficiencies ($p < 0.01$). Error bars represent ± SEM deviation with three replicates.

further, we explored the effects of lowering the max temperature to 37 °C and increasing the heat shock time to 45 seconds (optimal conditions shown in Fig. S3†). Fig. 3C shows that having a fast time constant of 0.5 (at 37 °C) yields a higher transformation efficiency (~3.5×10^6 CFU μg^{-1} for τ = 0.5 seconds; n = 3) on the device compared with the transformation performed in the tube (~1.2×10^6 CFU μg^{-1} for τ = 17 seconds; n = 3). We note that heat shock transformation has previously been implemented in microfluidics,[15,48] but to our knowledge, this is the first method to directly control the heat shock time constants to optimize transformation efficiency. Thus, we propose that this technique is a universal strategy for improving transformation efficiency, especially for transforming complex plasmids using microfluidics (as shown below).

Optimized DNA assembly and transformation for complex plasmids

In synthetic biology applications, it is common to assemble large multi-insert plasmids (usually on the order of >10 kb) that enable a biosynthetic pathway.[35,41,49,50] To demonstrate that DMF setups can be adapted for such a complex assembly and transformation, we used our optimized protocol to assemble and transform plasmids containing the five pathway genes that produce violacein.[35,51] Violacein is a purple pigment which exhibits several favorable properties relevant to a number of different health-based applications.[51,52] In addition, violacein is convenient for colorimetric screening of the correct pathway function and has been used in studies which demonstrate pathway optimization in *E. coli*[35] and in *S. cerevisiae*.[53] Hence, we selected this pathway to demonstrate the first large, multi-fragment assembly and transformation performed on DMF.

We developed an automated violacein assembly and transformation protocol on our rapid-prototype DMF platform. Apart from optimizing heat shock profiles for transformation, we discovered that the assembly product concentration is a major indicator for successful transformation (especially for complex plasmids like violacein). Increasing the DNA concentration is often used to ensure adequate numbers of transformants for screening; however, lower DNA concentrations are recommended for Golden Gate assembly reactions.[22,54] In addition, it is recommended that we dilute ligation products before transformation because components in the ligase reaction can negatively impact cells (see manufacturer protocols from Thermo Scientific[55] and NEB[56]). Hence, we investigated volume adjustments of assembly products performed on-device and compared the resulting colony numbers and transformation efficiencies (Fig. 4A). Starting with the sample droplets containing the pFAB assembly product, we used different volumes for transformation (depicted in Fig. S6†). We achieved this by removing part of the assembly reaction from the incubation area by electrode actuation. To limit competent cell dilution by the assembly product, we evaporated all samples to ~100 nL at 37 °C. Using less assembled products for transformations (either 0.2 or 0.1×)

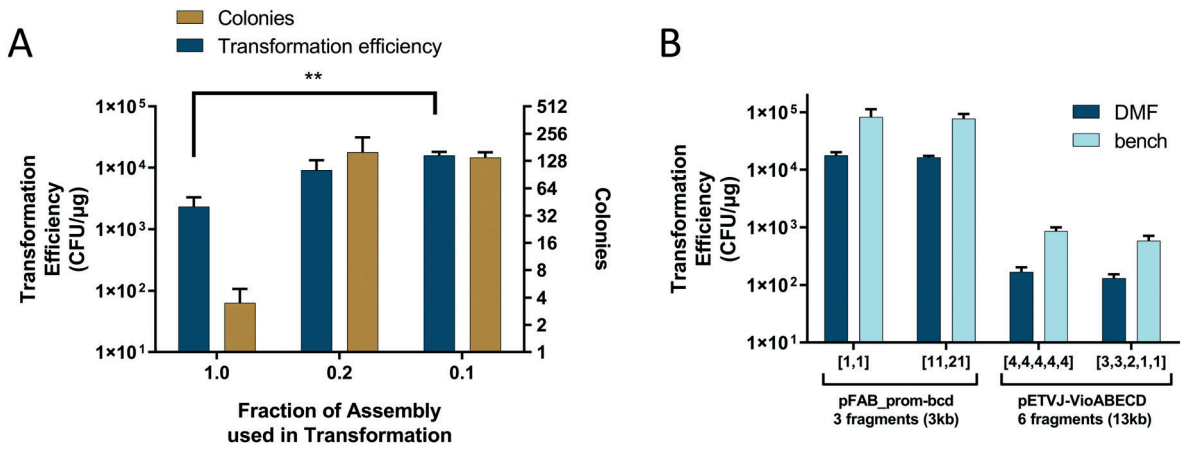

Fig. 4 Assembly and transformation for the violacein biosynthetic pathway. A) On-chip optimization of the assembly concentration used in transformation. This was done by either using the entire sample (1×), 1/5 of the sample (0.2×) by which a droplet was dispensed from the sample to be used for transformation, or 1/10 of the assembled product (0.1×), by which the sample was diluted with water and a single droplet was used for transformation. B) Small and large plasmid assembly and transformation performed on-chip using 25 temperature cycles and 0.2× of the assembled product. pFAB assemblies represent 3 fragments assembled into a 3 kb plasmid. pETM6-VIOABECD assemblies represent 6 fragments assembled into a 13 kb plasmid. Bracket numbers refer to the promoter and RBS variant used for the assembly – *e.g.*, [1,1] refers to promoter 1 and BCD 1 from the engineered library reported by Mutalik *et al.* (2013).[59] Similarly, for violacein samples, the numbers represent the promoters chosen for each gene cassette (ABECD) as per Jones *et al.* (2015)[35] – *e.g.*, for [4,4,4,4,4] each gene cassette possesses the consensus T7 promoter sequence.

significantly increased the efficiency ($\sim 10^4$ CFU μg^{-1}) compared with using the entire assembly mixture (1.0×; $\sim 10^2$ CFU μg^{-1}) performed on the device. The 0.2× and 0.1× products for transformation yielded the highest number of colonies, and were the most practical for obtaining transformants from the low-volume reactions.

Assembling Vio-parts required different promoters and gene fragments to be actuated on the common electrode track, we surveyed on-device assembly fidelity and cross-contamination on our device. We assembled and transformed triplicate samples of pFAB[1,1] and pFAB[11,21] on the device. From the Sanger sequencing results, we observe (1) that the fidelity of the sequence is highly preserved showing very few mutations (>98% correct for pFAB[1,1] and 100% for pFAB[11,21]) in three 100 bp regions centered on assembly junctions and (2) we did not observe any sequences from the other assembled samples (from the 12 colonies we randomly selected) suggesting that cross-contamination is minimal on our device (see the ESI† – Sequencing results).

After optimizing the concentration of the assembled product, we chose two pETVJ-VioABECD constructs (varied by gene cassette promoter strengths) and implemented our optimized protocol (thermal cycling, volume replenishment, and optimized heat shock protocol) and compared it with a benchtop protocol. Fig. 4B summarizes the data; as shown, violacein construct assemblies show comparable transformation efficiencies for the device and benchtop methods. The temperature and volume profiles and plate images for each assembly and transformation sample show precise control during the 25 cycles of thermocycling, which resulted in colony growth on the plates containing purple violacein colonies (Fig. S14†). All the selected colonies were verified by colony PCR, which shows the correct band sizes of the assembled junctions (Fig. S15†). Additionally, we transformed prepared plasmids into IPTG-induced BL21(DE3). In future work, we believe that this platform can be applied to other metabolic pathways, producing compounds such as alkaloids/opioids[57] that do not necessarily produce pigmented colonies. Regardless, adjusting the concentration of assembly reaction on-chip *via* evaporation and replenishment and tuning the heat shock profile to optimize transformation are key factors leading to successful construction of large constructs. Future improvements in device throughput (*e.g.*, using thin-film transistor based digital microfluidic devices[58]) will bring this method to the level of library construction necessary for applications in metabolic engineering.

Conclusion

In summary, this work shows the utility of rapid-prototyping technology to perform one-pot Golden Gate assembly and transformation of large, multi-fragment plasmids. The rapid prototyping process was greatly improved through optimization of the electrode design and modularity. To address sample evaporation, a volume replenishment system was implemented using a 3D printed syringe pump and impedance sensing infrastructure to maintain sample volumes which enabled 25 thermocycling steps to be performed on-chip. This significantly improved the efficiency of DNA assembly by facilitating longer incubation periods. Additionally, on-chip heat shock transformation was improved by investigating the thermodynamic heat shock profile and tailoring it to a digital microfluidic platform. Taken together, these improvements make our system the first DMF device capable of true one-pot Golden Gate

assembly and transformation, yielding the largest assemblies documented using microfluidics.

Author contributions

The research was designed by JMP, GS, and SCCS. All experiments and analysis were conducted by JMP, GS and SCCS. Biological and microfluidic methods were developed by JMP. Violacein constructs were designed and built by RJ and JMP. The mathematical modeling, simulations and controller software were done by JMP and GS. DMF device design and fabrication was done by JMP. The electrical and software systems used for DMF actuation were developed by GS and JMP. The TEC temperature control system was developed by GS and JMP. All authors wrote, revised, and reviewed the manuscript.

Conflicts of interest

There are no conflicts of interest to declare.

Acknowledgements

We thank the Natural Sciences and Engineering Research Council (NSERC), the Fonds de Recherche Nature et technologies (FRQNT), and the Canadian Foundation of Innovation (CFI) for funding. GS thanks the Concordia University Department of Electrical and Computer Engineering for FRS funding and the Department of Biology for academic resources. RJ thanks Mitacs for a Globalink Research Internship award. SCCS thanks Concordia University for a University Research Chair.

References

1 K. Müller, M. Ifversen, K. Kielsen, S. L. Petersen, Ö. Met and I. M. Svane, *Ugeskr. Laeg.*, 2019, **181**, 64–73.
2 R. A. Le Feuvre and N. S. Scrutton, *Synth. Syst. Biotechnol.*, 2018, **3**, 105–112.
3 C. L. Liu, T. Tian, J. Alonso-Gutierrez, B. Garabedian, S. Wang, E. E. K. Baidoo, V. Benites, Y. Chen, C. J. Petzold, P. D. Adams, J. D. Keasling, T. Tan and T. S. Lee, *Biotechnol. Biofuels*, 2018, **11**, 1–15.
4 S. R. Little, J. M. Perry, K. Samlali and S. C. C. Shih, in *Droplet Microfluidics*, 2020, pp. 193–222.
5 G. Linshiz, N. Stawski, G. Goyal, C. Bi, S. Poust, M. Sharma, V. Mutalik, J. D. Keasling and N. J. Hillson, *ACS Synth. Biol.*, 2014, **3**, 515–524.
6 W. G. Patrick, A. A. K. Nielsen, S. J. Keating, T. J. Levy, C.-W. Wang, J. J. Rivera, O. Mondragón-Palomino, P. A. Carr, C. A. Voigt, N. Oxman and D. S. Kong, *PLoS One*, 2015, **10**, e0143636.
7 G. Goyal, N. Elsbree, M. Fero, N. J. Hillson and G. Linshiz, *PLoS One*, 2020, **15**, 1–11.
8 Y. Khilko, P. D. Weyman, J. I. Glass, M. D. Adams, M. A. McNeil and P. B. Griffin, *BMC Biotechnol.*, 2018, **18**, 1–14.
9 Y. J. Liu, D. J. Yao, H. C. Lin, W. Y. Chang and H. Y. Chang, *J. Micromech. Microeng.*, 2008, **18**, 045017.
10 H.-C. Lin, Y.-J. Liu and D.-J. Yao, *J. Assoc. Lab. Autom.*, 2010, **15**, 210–215.
11 S. C. C. Shih, G. Goyal, P. W. Kim, N. Koutsoubelis, J. D. Keasling, P. D. Adams, N. J. Hillson and A. K. Singh, *ACS Synth. Biol.*, 2015, **4**, 1151–1164.
12 N. J. Hillson, R. D. Rosengarten and J. D. Keasling, *ACS Synth. Biol.*, 2012, **1**, 14–21.
13 D. I. Walsh, M. Pavan, L. Ortiz, S. Wick, J. Bobrow, N. J. Guido, S. Leinicke, D. Fu, S. Pandit, L. Qin, P. A. Carr and D. Densmore, *SLAS Technol.*, 2019, **24**, 282–290.
14 P. Kumar, A. Nagarajan and P. D. Uchil, *Cold Spring Harb. Protoc.*, 2019, **2019**, 519–525.
15 P. C. Gach, S. C. C. Shih, J. Sustarich, J. D. Keasling, N. J. Hillson, P. D. Adams and A. K. Singh, *ACS Synth. Biol.*, 2016, **5**, 426–433.
16 S. H. Au, S. C. C. Shih and A. R. Wheeler, *Biomed. Microdevices*, 2011, **13**, 41–50.
17 E. Moazami, J. M. Perry, G. Soffer, M. C. Husser and S. C. C. Shih, *Anal. Chem.*, 2019, **91**, 5159–5168.
18 P. A. Garcia, Z. Ge, J. L. Moran and C. R. Buie, *Sci. Rep.*, 2016, **6**, 21238.
19 P. A. Garcia, Z. Ge, L. E. Kelley, S. J. Holcomb and C. R. Buie, *Lab Chip*, 2017, **17**, 490–500.
20 A. C. Madison, M. W. Royal, F. Vigneault, L. Chen, P. B. Griffin, M. Horowitz, G. M. Church and R. B. Fair, *ACS Synth. Biol.*, 2017, **6**, 1701–1709.
21 M. Szostková and D. Horáková, *Bioelectrochem. Bioenerg.*, 1998, **47**, 319–323.
22 C. Engler, R. Gruetzner, R. Kandzia and S. Marillonnet, *PLoS One*, 2009, **4**, e5553.
23 E. Weber, C. Engler, R. Gruetzner, S. Werner and S. Marillonnet, *PLoS One*, 2011, **6**, e16765.
24 S. V. Iverson, T. L. Haddock, J. Beal and D. M. Densmore, *ACS Synth. Biol.*, 2016, **5**, 99–103.
25 H. Sinha, A. B. V. Quach, P. Q. N. Vo and S. C. C. Shih, *Lab Chip*, 2018, **18**, 2300–2312.
26 M. C. Husser, P. Q. N. Vo, H. Sinha, F. Ahmadi and S. C. C. Shih, *ACS Synth. Biol.*, 2018, **7**, 933–944.
27 S. C. C. Shih, H. Yang, M. J. Jebrail, R. Fobel, N. McIntosh, O. Y. Al-Dirbashi, P. Chakraborty and A. R. Wheeler, *Anal. Chem.*, 2012, **84**, 3731–3738.
28 M. Abdelgawad and A. R. Wheeler, *Adv. Mater.*, 2007, **19**, 133–137.
29 C. Dixon, A. H. C. Ng, R. Fobel, M. B. Miltenburg and A. R. Wheeler, *Lab Chip*, 2016, **16**, 4560–4568.
30 V. Soum, Y. Kim, S. Park, M. Chuong, S. Ryu, S. Lee, G. Tanev, J. Madsen, O.-S. Kwon and K. Shin, *Micromachines*, 2019, **10**, 109.
31 S. Kosuri and G. M. Church, *Nat. Methods*, 2014, **11**, 499–507.
32 M. Abdelgawad and A. R. Wheeler, *Microfluid. Nanofluid.*, 2008, **4**, 349–355.
33 V. Jain, T. P. Raj, R. Deshmukh and R. Patrikar, *Microsyst. Technol.*, 2017, **23**, 389–397.
34 A. H. C. Ng, R. Fobel, C. Fobel, J. Lamanna, D. G. Rackus, A. Summers, C. Dixon, M. D. M. Dryden, C. Lam, M. Ho, N. S.

Mufti, V. Lee, M. A. M. Asri, E. A. Sykes, M. D. Chamberlain, R. Joseph, M. Ope, H. M. Scobie, A. Knipes, P. A. Rota, N. Marano, P. M. Chege, M. Njuguna, R. Nzunza, N. Kisangau, J. Kiogora, M. Karuingi, J. W. Burton, P. Borus, E. Lam and A. R. Wheeler, *Sci. Transl. Med.*, 2018, **10**, eaar6076.

35 J. A. Jones, V. R. Vernacchio, D. M. Lachance, M. Lebovich, L. Fu, A. N. Shirke, V. L. Schultz, B. Cress, R. J. Linhardt and M. A. G. Koffas, *Sci. Rep.*, 2015, **5**, 1–10.

36 P. Q. N. Vo, M. C. Husser, F. Ahmadi, H. Sinha and S. C. C. Shih, *Lab Chip*, 2017, **17**, 3437–3446.

37 J. Gong and C. J. Kim, *J. Microelectromech. Syst.*, 2008, **17**, 257–264.

38 L. M. Y. Leclerc, G. Soffer, D. H. Kwan and S. C. C. Shih, *Biomicrofluidics*, 2019, **13**, 034106.

39 S. C. C. Shih, I. Barbulovic-Nad, X. Yang, R. Fobel and A. R. Wheeler, *Biosens. Bioelectron.*, 2013, **42**, 314–320.

40 M. E. Lee, W. C. DeLoache, B. Cervantes and J. E. Dueber, *ACS Synth. Biol.*, 2015, **4**, 975–986.

41 H. E. Lai, S. Moore, K. Polizzi and P. Freemont, *Methods Mol. Biol.*, 2018, **1772**, 429–444.

42 R. Sista, Z. Hua, P. Thwar, A. Sudarsan, V. Srinivasan, A. Eckhardt, M. Pollack and V. Pamula, *Lab Chip*, 2008, **8**, 2091.

43 S. Kalsi, M. Valiadi, M. N. Tsaloglou, L. Parry-Jones, A. Jacobs, R. Watson, C. Turner, R. Amos, B. Hadwen, J. Buse, C. Brown, M. Sutton and H. Morgan, *Lab Chip*, 2015, **15**, 3065–3075.

44 M. Kühnemund, D. Witters, M. Nilsson and J. Lammertyn, *Lab Chip*, 2014, **14**, 2983–2992.

45 C. Zhang, Y. Su, S. Hu, K. Jin, Y. Jie, W. Li, A. Nathan and H. Ma, *ACS Omega*, 2020, **5**, 5098–5104.

46 S. Sadeghi, H. Ding, G. J. Shah, S. Chen, P. Y. Keng, C.-J. Kim and R. M. van Dam, *Anal. Chem.*, 2012, **84**, 1915–1923.

47 D. Brassard, L. Malic, F. Normandin, M. Tabrizian and T. Veres, *Lab Chip*, 2008, **8**, 1342–1349.

48 J. Sha, Y. Wang, J. Wang, W. Liu, Q. Tu, A. Liu, L. Wang and J. Wang, *Anal. Methods*, 2011, **3**, 1988–1994.

49 C. M. Denby, R. A. Li, V. T. Vu, Z. Costello, W. Lin, L. J. G. Chan, J. Williams, B. Donaldson, C. W. Bamforth, C. J. Petzold, H. V. Scheller, H. G. Martin and J. D. Keasling, *Nat. Commun.*, 2018, **9**, 965.

50 X. Luo, M. A. Reiter, L. d'Espaux, J. Wong, C. M. Denby, A. Lechner, Y. Zhang, A. T. Grzybowski, S. Harth, W. Lin, H. Lee, C. Yu, J. Shin, K. Deng, V. T. Benites, G. Wang, E. E. K. Baidoo, Y. Chen, I. Dev, C. J. Petzold and J. D. Keasling, *Nature*, 2019, **567**, 123–126.

51 L. Masuelli, F. Pantanella, G. La Regina, M. Benvenuto, M. Fantini, R. Mattera, E. Di Stefano, M. Mattei, R. Silvestri, S. Schippa, V. Manzari, A. Modesti and R. Bei, *Tumor Biol.*, 2016, **37**, 3705–3717.

52 L. L. Kodach, C. L. Bos, N. Durán, M. P. Peppelenbosch, C. V. Ferreira and J. C. H. Hardwick, *Carcinogenesis*, 2006, **27**, 508–516.

53 M. E. Lee, A. Aswani, A. S. Han, C. J. Tomlin and J. E. Dueber, *Nucleic Acids Res.*, 2013, **41**, 10668–10678.

54 C. Engler, R. Kandzia and S. Marillonnet, *PLoS One*, 2008, **3**, e3647.

55 Thermo Scientific, *DNA Insert Ligation (sticky-end and blunt-end) into Vector DNA*, https://tools.thermofisher.com/content/sfs/manuals/MAN0011906_DNAsert_Ligation_Vector_DNA_UG.pdf.

56 NEB, *Ligation Protocol with T4 DNA Ligase (M0202)*, https://international.neb.com/protocols/0001/01/01/dna-ligation-with-t4-dna-ligase-m0202, (accessed 19 April 2021).

57 M. E. Pyne, K. Kevvai, P. S. Grewal, L. Narcross, B. Choi, L. Bourgeois, J. E. Dueber and V. J. J. Martin, *Nat. Commun.*, 2020, **11**, 1–10.

58 S. Anderson, B. Hadwen and C. Brown, *Lab Chip*, 2021, **21**, 962–975.

59 V. K. Mutalik, J. C. Guimaraes, G. Cambray, C. Lam, M. J. Christoffersen, Q. A. Mai, A. B. Tran, M. Paull, J. D. Keasling, A. P. Arkin and D. Endy, *Nat. Methods*, 2013, **10**, 354–360.